Applied Catalysis B: Environment and Energy 354 (2024) 124152

Contents lists available at ScienceDirect

Applied Catalysis B: Environment and Energy

journal homepage: www.elsevier.com/locate/apcatb

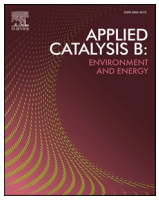

Silica-assisted Pt_1/CeO_2 single-atom catalyst for enhancing the catalytic combustion performance of VOCs by inducing H_2O activation

Siyi Ma [a,b], Fang Dong [a,*], Shixing Wu [a,b], Weitong Ling [c], Weiliang Han [a], Weigao Han [a], Zhicheng Tang [a,*]

[a] National Engineering Research Center for Fine Petrochemical Intermediates, State Key Laboratory for Oxo Synthesis and Selective Oxidation, Lanzhou Institute of Chemical Physics, Chinese Academy of Sciences, Lanzhou 730000, China
[b] University of Chinese Academy of Sciences, Beijing 100039, China
[c] State Key Laboratory of Fine Chemicals, Key Laboratory of Industrial Ecology and Environmental Engineering (MOE), School of Environmental Science and Technology Dalian University of Technology, Dalian 116024, China

ARTICLE INFO

Keywords:
Pt single atoms
Core-shell structure
SiO_2
Water resistance
Catalytic oxidation

ABSTRACT

Due to the competitive adsorption of water and reactants at the active sites, especially the water toxicity of platinum-based single-atom catalysts, it is of great importance to improve the low-temperature activity and the water resistance of catalysts for the catalytic combustion of benzene. In this work, it was found that constructing a SiO_2 shell layer on the catalyst not only "immobilized" the Pt single atoms, but also effectively weakened the adsorption of H_2O on the Pt active sites, which resulted in excellent water resistance of the Pt single-atom catalysts. The comprehensive characterization results demonstrated that the participation of water molecules in the catalytic oxidation reaction of benzene could be effectively promoted by enhancing the strong metal-support interactions (SMSI) at the core-shell interface, which would change the electronic structure of the catalyst surface. As a result, the $Pt_1/CeO_2@SiO_2$-4 catalyst with a Pt-O-Si active interface exhibits good activity (T = 190 °C) as well as excellent water resistance under the wet condition (10 vol%). This project provides a promising strategy for the design of Pt-based core-shell catalysts with excellent water resistance.

1. Introduction

Volatile organic compounds (VOCs) are one of the gaseous pollutants that affect the atmospheric environment and jeopardize human health. VOCs comprise a range of complicated chemicals that make them difficult to destroy and extensively prevalent in the atmosphere, making their eradication an essential undertaking. Catalytic oxidation is one of the most effective technologies [1,2] for controlling the emissions of VOCs due to the advantages of non-secondary pollution, high conversion efficiency, and so on. At low temperatures, precious metal catalysts may now achieve full combustion of VOCs. However, the expensive cost of precious metals is impeding their growth. Generally speaking, the size and the dispersion of metal particles are the key factors in determining their catalytic performances [3]. Therefore, single-atom catalysts have already achieved remarkable results in catalysis with their high atom utilization and good coordination environments [4–8]. However, single-atom catalysts (SACs) are still in the initial stage of development in the field of catalytic combustion of VOCs, so the development of single-atom catalysts suitable for catalytic combustion of VOCs is an inevitable and beneficial research direction.

The key performance indicators such as efficient catalytic activity, durability, or toxicity resistance are essential for practical single-atom catalysts, especially applied to the catalytic oxidation of VOCs [9–11]. The platinum-based catalysts with excellent catalytic activity are widely used in VOCs, but due to their strong adsorption, they can adsorb water vapor, sulfur, and other substances [12]. Therefore, for the complex VOCs feedstock, platinum single-atom catalysts would be susceptible to poisoning by exposing more active sites and coming into contact with H_2O and other substances on a large scale [13]. Consequently, studies have been devoted to improving the toxicity resistance (such as water toxicity) of noble metal single-atom catalysts in the field of catalytic combustion of VOCs [14]. Normally, the introduced water can cause charge transfer with the noble metal, which produces less active $M\text{-}(OH)_x$ or inhibits the active center [15], leading to the deactivation of the catalysts. Subsequently, various strategies have been devised to improve the water resistance of catalysts. In order to successfully

* Corresponding authors.
E-mail addresses: dongfang@licp.cas.cn (F. Dong), tangzhicheng@licp.cas.cn (Z. Tang).

https://doi.org/10.1016/j.apcatb.2024.124152
Received 5 February 2024; Received in revised form 17 April 2024; Accepted 1 May 2024
Available online 4 May 2024

prevent the competitive adsorption of H_2O with the reactants, Wang et al. [12] used WO_3 aggregation over the Pt-3W/SO_4^{2-}-ZrO_2 sample to form strong metal-support interactions (SMSI), which was further enhanced by SO_4^{2-}-ZrO_2. So the enhanced SMSI could be beneficial for weakening the water vapor adsorption on the active sites and thus effectively inhibit the competitive adsorption of H_2O with the reactants. Wang et al. [16] designed the Pt_1/CeO_2 single-atom catalyst in which water could directly participate in CO oxidation. The reaction of CO at the Pt_1-top with the hydroxyl group from water dissociated at the CeO_2 surface produced a carboxyl intermediate, which was dehydrogenated with the help of lattice hydroxyl groups to produce CO_2 and water, realizing the water-mediated Mars-van Krevelen (MvK) mechanism. Li et al. [2] designed an Al_2O_3@Pd-CoAlO core-shell sample, which showed excellent hydrothermal stability of the catalyst due to the uniform distribution of Pd-CoAlO nanosheets and the strong interactions between Pd-CoAlO nanosheets and Al_2O_3 support. In sum, the approaches for creating single-atom catalysts resistant to toxicity are mainly related to the interaction between the active sites and the supports, and the core-shell structure is one of the effective initiatives to enhance the water resistance of catalysts. The core-shell structure can realize the charge transfer at the metal-oxide interface [17,18], and the alteration of the local electronic structure contributes to the modulation of the catalytic performance [19], which significantly improves the adsorption and activation of reactants. Therefore, core-shell catalysts can effectively enhance the metal-carrier interaction (MSI).

In addition, the core-shell material not only effectively enhances the water resistant of the metal catalysts, but also effectively restricts the single-atom active sites to avoid migration and aggregation of the noble metals. Kim et al. [20] demonstrated with the help of HAADF-STEM, XANES, and XPS techniques that SiO_2 coatings could mitigate the agglomeration behavior of Pt species during thermal activation. Additionally, Peng et al. [21] reported a core-shell confinement strategy that could effectively protect the active site from sintering with the help of silicon shells. From the HAADF-STEM images, the Pd-Ce core was completely encapsulated in the silica shell. Therefore, the core-shell structure can meet the requirements of fixing single atoms while effectively shielding direct contact between water molecules and active sites, to prevent catalyst poisoning. In general, the electronic structure of the catalysts can be induced with the help of interactions between strong metals and reducing supports [22]. Appropriate strong metal-support interactions (SMSI) are helpful to the enhancement of the active interface and efficiently regulate the strength of the local charge transfer [23,24]. Consequently, creating and researching catalysts with appropriate SMSI strength that can drive structural changes on the surface of the core shell is difficult.

Herein, we proposed a SiO_2 shell-assisted strategy to construct a Pt-O-Si active interface by covering a layer of SiO_2 on the surface of Pt_1/CeO_2. It not only realized the effective immobilization and isolation of Pt single atoms to avoid agglomeration but also helped to improve the influence of water molecules on the active sites. The single-atom catalyst (Pt_1/CeO_2@SiO_2-4) exhibited unique water resistance and had excellent low-temperature catalytic activity in humid environments. Various characterizations confirmed that the Pt-O-Si active interface helped to induce H_2O and O_2 activation [25], which increased the anti-poisoning ability of the catalysts (Pt_1/CeO_2@SiO_2-x). Moreover, the mechanistic studies showed that the core-shell structure altered the reaction mechanism pathway and the oxygen activation route of Pt-CeO_2-based catalysts in the aqueous environment. It also suggested that the altered reaction mechanism and the generation of new reactive oxygen species were the main reasons for the excellent water resistance of the Pt_1/CeO_2@SiO_2-x catalysts. This work provides a research basis for the design of Pt single-atom catalysts with excellent hydrothermal stability.

2. Experimental contents

Synthesis of 0.3% Pt_1/CeO_2@SiO_2-x. 1.0 g of CeO_2 powder was dispersed in methanol and 0.40 mL of H_2PtCl_4 solution (38.6 mmol/L) was added to an aqueous solution of 0.004 g of PVA (noble metal/PVA mass ratio = 1.0:1.2). Subsequently, the solution containing Pt precursor was added dropwise to the CeO_2 solution and stirred vigorously for 3 h under an ice bath. Next, a solution of $NaBH_4$ (0.06 g) dissolved in water was slowly dripped into the mixed solution and stirred for 1 h. Later, different volumes of TEOS were added to a methanol solution containing $Pt^{\delta+}/CeO_2$, stirred for 48 h, and then the solutions were dried at 60 °C. Finally, the solid ($Pt^{\delta+}/CeO_2$) was calcined from room temperature to 450 °C at a ramp rate of 1 °C/min and kept for 2 h to obtain the 0.3 wt% Pt_1/CeO_2@SiO_2-x catalysts (the theoretical SiO_2 loadings (x) were 2, 4 and 5 wt%, respectively).

Preparation, equations, and performance testing of single-atom catalysts (CeO_2 and Pt_1/CeO_2) were described in Supplementary Information (SI). And the details of other characterization techniques, such as transmission electron microscopy (TEM), scanning electron microscope (SEM), Aberration-corrected high-angle annular dark-field scanning transmission electron microscopy (AC-HAADF-STEM), X-ray absorption near-edge structure (XANES) spectra, extended X-ray absorption fine structure (EXAFS) fitting, X-ray diffraction (XRD), Raman spectroscopy, N_2 adsorption-desorption, X-ray photoelectron spectroscopy (XPS), O_2-Temperature program desorption (O_2-TPD), He-Temperature program desorption (He-TPD), NH_3-Temperature program desorption (NH_3-TPD), H_2-Temperature program reduction (H_2-TPR), in situ diffuse reflectance infrared Fourier transform spectroscopy (DRIFTS), were also recorded in the SI.

3. Results

3.1. Physical properties of catalysts

In Fig. 1a, to prepare water-resistant single-atom catalysts, we first utilized a CeO_2 support to realize the anchoring of Pt single atoms by the PVA-protected reduction method, and then covered the CeO_2 surface of the impregnated precursors with a certain thickness of SiO_2 shell, so as to enable the Pt single atoms to be immobilized and segregated during the roasting and thermal decomposition processes to reduce the occurrence of agglomeration. SEM and TEM were used to characterize the micro-morphology of the samples (Fig. S1). In Fig. S1a, b, it can be found that CeO_2 mainly exhibited a rod-like structure. Meanwhile, changing the mass of the SiO_2 shell, the morphology of the samples did not alter significantly (Fig. S1c-h). Besides, Fig. 1b, e showed that the Pt_1/CeO_2@SiO_2-4 sample appeared a clear SiO_2 film on the surface, compared to the Pt_1/CeO_2 sample. It can also be demonstrated in Fig. S1i-l that the outer layer of the rods gradually revealed a transparent SiO_2 film as the SiO_2 content increased. HAADF-STEM showed the high dispersion of Pt on the Pt_1/CeO_2 sample (Fig. 1c) and the Pt_1/CeO_2@SiO_2-4 sample (Fig. 1f). The distribution of the elements was derived from the EDS data (Figs. 1d and 1g), which showed that the Pt elements did not significantly cluster. It is worth mentioning that Pt elements were relatively dispersed on the Pt_1/CeO_2@SiO_2-4 sample compared to the Pt_1/CeO_2 sample, which suggested that the introduction of the SiO_2 capping played a protective role for the Pt species, thus effectively dispersing and isolating the Pt single atoms. Subsequently, the samples were tested by in situ DRIFTS of CO adsorption, as shown in Fig. 2a. Under the CO flow, there was no obvious peak present at ~ 1840 cm^{-1} or 2060 cm^{-1}, indicating that Pt nanoparticles were not evidently present in the Pt_1/CeO_2 and Pt_1/CeO_2@SiO_2-x samples. In addition, the four samples showed two bands at ~2172 cm^{-1} and ~2117 cm^{-1}, which attributed to the CO gas phase and CO adsorbed on Pt single sites, respectively [26,27]. During the argon purge, the intensity of peaks gradually decreased due to the removal of physically adsorbed CO. It was noteworthy that after a period of Ar purge, the two residual CO adsorption peaks still survived on the catalysts, indicating that a degree of chemical interaction between the catalysts and CO [28].

The XAS test could clarify the coordination environment of Pt

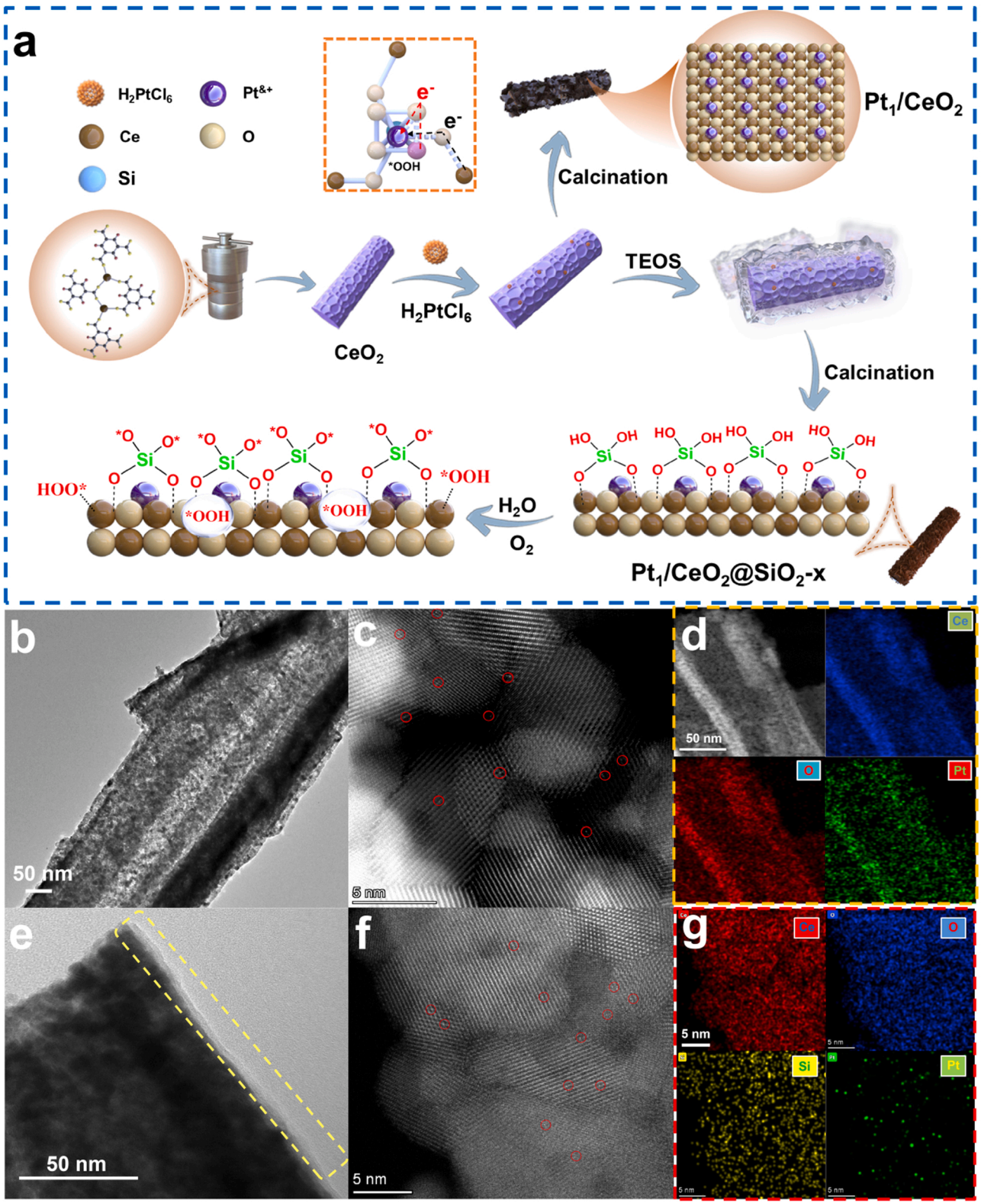

Fig. 1. The preparation of Pt_1/CeO_2 and $Pt_1/CeO_2@SiO_2$-x catalysts (a). The TEM diagram (b), the AC-HAADF-STEM (c), and the EDS with 50 nm (d) of the Pt_1/CeO_2 sample. The TEM diagram (e), the AC-HAADF-STEM (f), and the EDS with 5 nm (g) of the $Pt_1/CeO_2@SiO_2$-4 sample.

elements. The XANES spectra of the $Pt_1/CeO_2@SiO_2$-4 sample had similar adsorption energies at 11568 eV as that of PtO_2 (Fig. 2b), suggesting that the average valence of Pt elements was in the range between 0 and 4+ valence. From the EXAFS curves (Fig. 2c, d, Fig. S2a-c), the Pt-O bond located at 2.013 Å in the first coordination shell layer was the main component of the bond on the $Pt_1/CeO_2@SiO_2$-4 sample, and the number of Pt-O coordination was close to the tetra-coordination. In addition, a few Pt-O-Pt and Pt-O-Ce scattering signals could be detected in the second shell layer, and the Pt-coordinated structure was evidenced by the good match between the model and the experimental k-

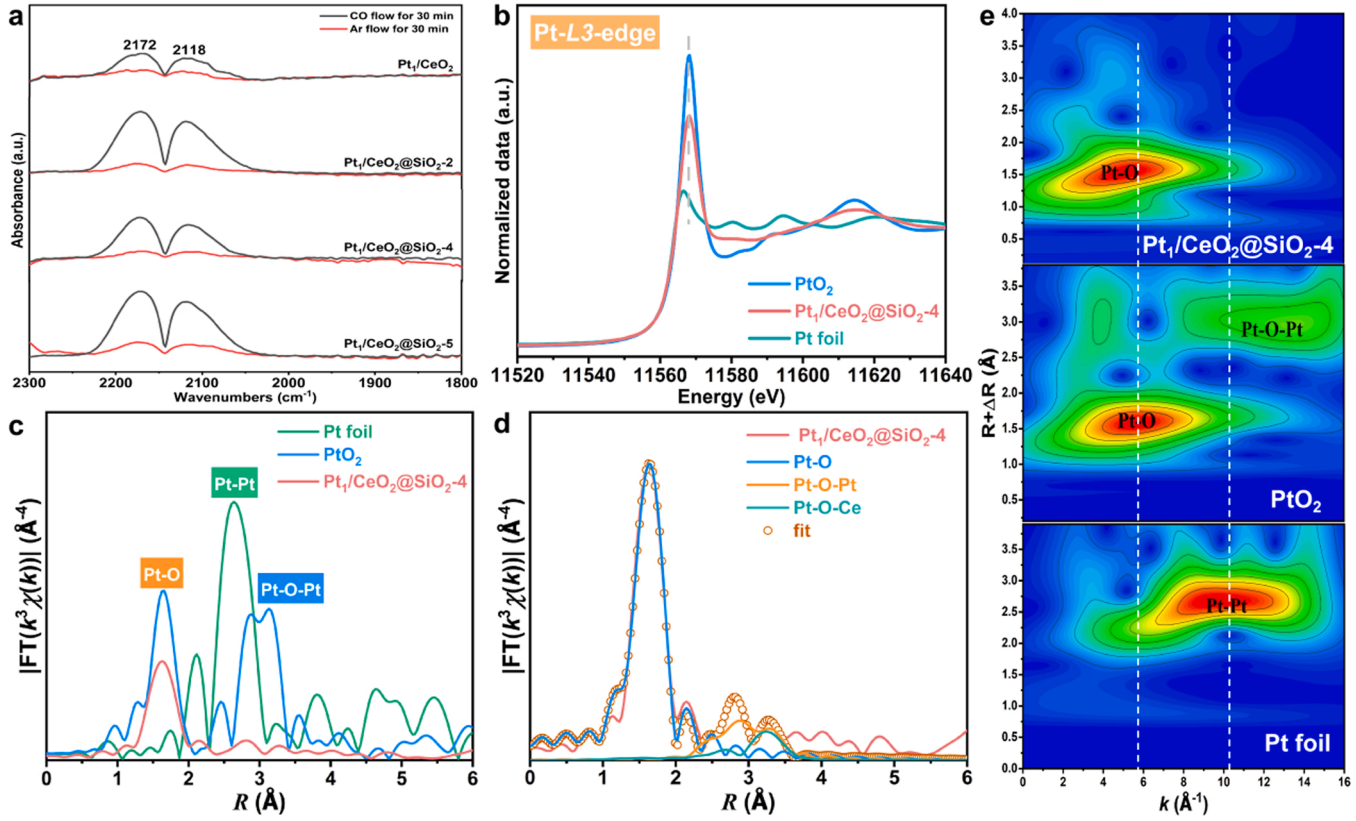

Fig. 2. In situ DRIFTS of CO adsorption and desorption at 50 °C on the samples (a). The XANES spectra of Pt_1/CeO_2@SiO_2-4 (b), the EXAFS magnitude of the Fourier transformed k^2-weighted χ(k) data of Pt_1/CeO_2@SiO_2-4, PtO_2 and Pt foil at the Pt L_3-edge (c), the fitted EXAFS magnitude of the data of the Pt_1/CeO_2@SiO_2-4 sample (d), and the Wavelet transform plots of Pt_1/CeO_2@SiO_2-4, PtO_2 and Pt foil (e).

space and r-space curves [29]. The results of each data were statistically presented in Table S1. Overall, the Pt atoms were still mainly in the form of single-atom dispersion. The EXAFS data showed that the sample exhibited two weak peaks near 3 Å, which were found to be the result of the combined effect of Pt-O-Pt and Pt-O-Ce by simulation analysis. From the wavelet transform diagram (Fig. 2e), it can also be demonstrated that the Pt-O bond was mainly present on the Pt_1/CeO_2@SiO_2-4 sample, but there were no particularly obvious Pt-O-Pt and Pt-O-Ce signals, which may be due to the weak signals of the Pt-O-Pt and Pt-O-Ce. Combined with the HAADF-STEM images, in situ DRIFTS of CO adsorption, and XAS results, Pt species mainly existed as Pt single atoms (Pt SAs) and also verified the feasibility of the Pt SAC preparation method. Additionally, the XRD spectra (Fig. S2d) showed that the crystal structures of each catalyst conformed to the XRD standard card of CeO_2 (JCPDS 34–0394). Furthermore, the EDS result confirmed that a high degree of Si dispersion had been obtained over the catalysts, as seen by the absence of the matching Si peaks in Fig. S2d. Moreover, it was difficult to measure the diffraction peaks of the Pt element on the catalysts due to the formation of Pt single atoms. Interestingly, the addition of silicon reduced the intensity of the diffraction peaks of the catalysts, which was thought to be a change in the crystallinity of CeO_2. The change may be related to the fact that an interaction between Si and Ce species occurred, which suppressed the diffraction of the CeO_2 lattice. Naturally, the addition of SiO_2 also affected the specific surface area and the pore structure properties of each catalyst, which in turn could affect the catalytic performance of the catalysts (Table S2 and Fig. S2e). Compared to the Pt_1/CeO_2 sample, the Pt_1/CeO_2@SiO_2-x samples showed a significant decrease in pore size, which may be related to the formation of the SiO_2 capping layer. However, the specific surface area of the Pt_1/CeO_2@SiO_2-x samples showed the opposite trend. The results proved that the SiO_2 covering layer blocked part of the pore channels. Each sample showed a typical type IV nitrogen adsorption-desorption isotherm with a hysteresis return line (Fig. S2f).

3.2. Catalytic performance of catalysts

Next, activity tests were conducted for each catalyst (Fig. 3a-c). From Fig. 3a, it is clear that the T_{90} of Pt_1/CeO_2 and Pt_1/CeO_2@SiO_2-2 catalysts were 180 °C, while the activity of Pt_1/CeO_2@SiO_2-4 (T_{90} = 200 °C) and Pt_1/CeO_2@SiO_2-5 (T_{90} = 220 °C) catalysts were gradually decreasing. There was a decreasing trend in the activity of the catalysts with the increase in silicon content. Fig. 3b further demonstrated the effect of 10 vol% H_2O on benzene activity over each catalyst. Naturally, the inhibition of water vapor on the Pt_1/CeO_2 catalyst was the most obvious, especially the T_{90} increased from 180 °C to 220 °C. The effect of H_2O on benzene conversion was negligible over the Pt_1/CeO_2@SiO_2-4 catalyst which showed excellent water-resistant activity. In addition, we also investigated the activity of each catalyst after the end of water passage (Fig. 3c). It is obvious that the activities of the Pt_1/CeO_2@SiO_2-x samples after steam treatment were enhanced to a certain extent. When combined with the activity plots of Pt_1/CeO_2@SiO_2-4 catalyst and the Pt_1/CeO_2 catalyst before and after the passage of water (Fig. S3), the T_{90} of Pt_1/CeO_2@SiO_2-4 catalyst was reduced from 200 °C to 190 °C, and the T_{50} was reduced from 188 °C to 165 °C, which clearly confirmed the existence of a significant increase in the activity of Pt_1/CeO_2@SiO_2-4 catalyst after water resistance.

Meanwhile, to validate the activities of the Pt_1/CeO_2@SiO_2-4 catalyst before and after water passage (the catalyst after passing water was named u-Pt_1/CeO_2@SiO_2-4), a kinetic study was carried out (Fig. 3d-f). We chose the temperature points where the benzene conversion was below 20% to calculate the activation energy (E_a) of the catalysts. The apparent E_a of water was not considered in this case. As shown in Fig. 3d,

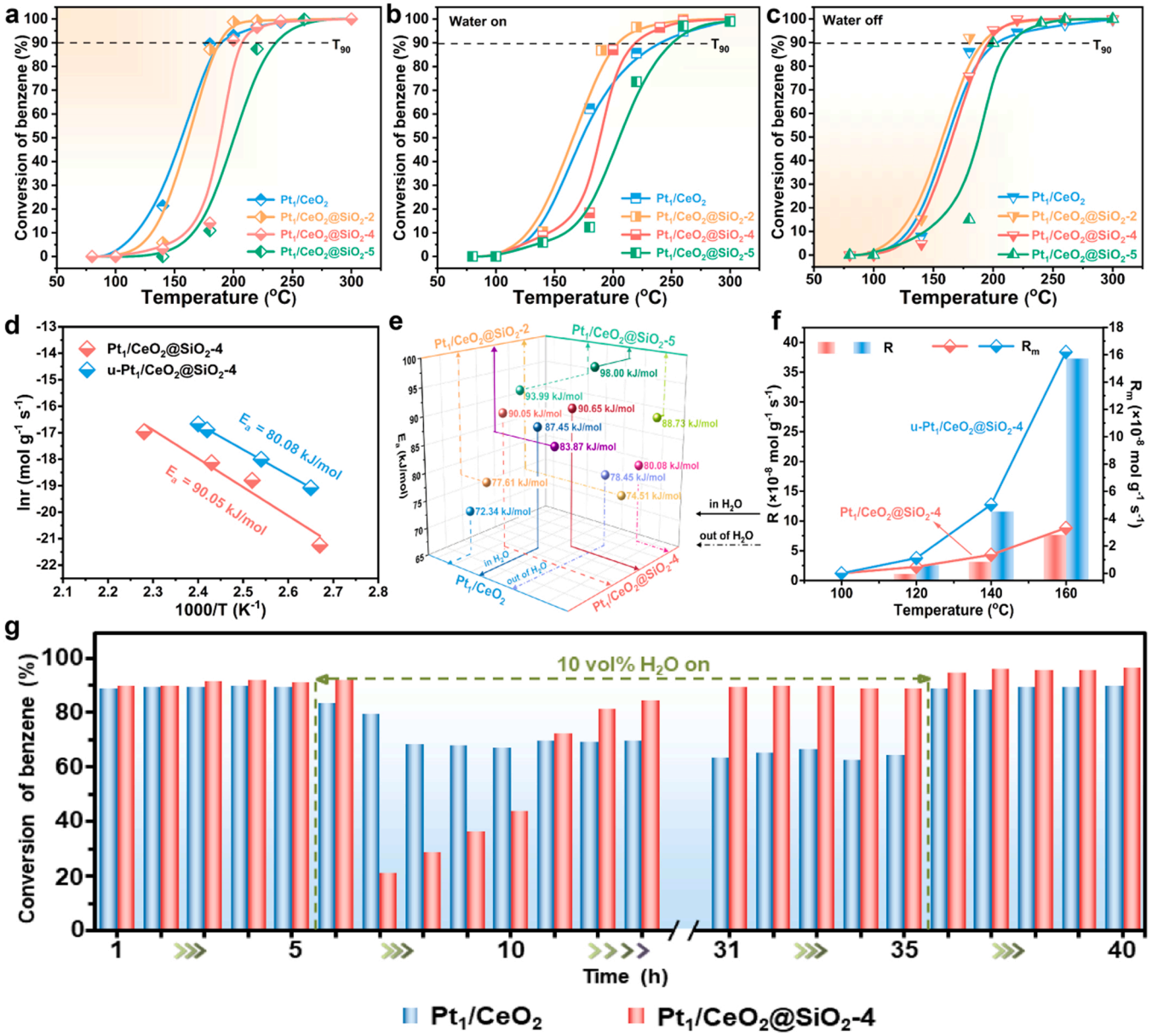

Fig. 3. The activity of fresh catalysts (a), the activity of catalysts within 10 vol% H_2O (b), and the activity of catalysts after water passage (c). The activation energies of $Pt_1/CeO_2@SiO_2$-4 and u-$Pt_1/CeO_2@SiO_2$-4 catalysts (d). The activation energies of all catalysts (e) in the presence and absence of H_2O. The reaction rates (R) and mass rates (R_m) of benzene conversion at different temperatures (f). Effect of water vapor (10 vol%) on the catalytic activity of Pt_1/CeO_2 and $Pt_1/CeO_2@SiO_2$-4 catalysts (g) for benzene combustion at WHSV = 30000 mL•g^{-1}•h^{-1}.

the E_a values of $Pt_1/CeO_2@SiO_2$-4 catalyst decreased from 90.05 to 80.08 kJ/mol. It also corresponded to the activity of the catalysts, and a smaller E_a value would show better catalytic activity. Besides, the catalysts in wet air were significantly higher than those in dry air (Fig. 3e). For the Pt_1/CeO_2 catalyst, the introduction of water increased the E_a value from 72.34 to 87.45 kJ/mol, while for the $Pt_1/CeO_2@SiO_2$-4 catalyst in wet air, the E_a was increased from 90.05 to 91.44 kJ/mol. Clearly, the impact of water on the Pt_1/CeO_2 single-atom catalyst was more significant. Additionally, the E_a values of the $Pt_1/CeO_2@SiO_2$-x catalysts were lower than those of the catalysts without water treatment after the water cut off. From Fig. 3f, it could be seen that the R and R_m values of the $Pt_1/CeO_2@SiO_2$-4 catalysts after water resistance were much larger than those of the non-water-treated $Pt_1/CeO_2@SiO_2$-4 catalyst. Dong et al. [25] found that the Pd-SiO_2 active interface promoted the activation of O_2 and H_2O, resulting in the generation of active oxygen species co-promoting the oxidation of formaldehyde. It was suggested that over the $Pt_1/CeO_2@SiO_2$-4 catalyst, water may form certain active species on the core-shell interface and promote the benzene decomposition reaction. Furthermore, the combination of activity and water resistance suggested that low temperatures may be more conducive to the production of active species.

In view of the better activity of water resistance of the $Pt_1/CeO_2@SiO_2$-4 catalyst, we performed water resistance tests with 30 h in the absence of 10 vol% water vapor to investigate the impact of water on the catalytic performance of the catalysts (Fig. 3g). From the water-resistance plots (Fig. 3g), it could be seen that the benzene conversion over the Pt_1/CeO_2 catalyst decreased by about 30% after the introduction of water, but it was recovered to the initial value when the water vapor was cut off. The benzene conversion over the $Pt_1/CeO_2@SiO_2$-4 catalyst decreased dramatically from 90% to 20% under the humid environment. However, with the prolongation of the time for water vapor addition, the benzene conversion gradually recovered to about

87% and maintained for at least 20 h, and the catalytic activity even exceeded the initial benzene conversion after cutting off the water vapor. The above results suggested that there might be some voids in the SiO_2 shells that may be permeable, leading to competitive adsorption of water molecules with benzene molecules at the initial stage of water introduction. Nevertheless, it may be due to the presence of silicon that the superior water resistance of the $Pt_1/CeO_2@SiO_2$-4 catalyst began to emerge after a brief competitive adsorption phenomenon occurred. In addition, the pore size of the Pt_1/CeO_2 catalyst was 11.53 nm, indicating that the catalyst would embed more water molecules and compete with benzene molecules for adsorption, resulting in a significant decrease in the water resistance of the Pt_1/CeO_2 catalyst. Up to now, the results showed that the $Pt_1/CeO_2@SiO_2$-4 catalyst displayed superior water resistance than the Pt_1/CeO_2 catalyst. To verify the reliability of the water-resistance result of the $Pt_1/CeO_2@SiO_2$-4 catalyst, the water-resistance tests were performed on the catalysts with different thicknesses of the silicon layer, and the results were shown in Fig. S4. The $Pt_1/CeO_2@SiO_2$-x catalysts showed good thermal stability without any deactivation in the absence of water vapor. After the introduction of water vapor (10 vol%), the stability of the catalysts was tested for 30 h. Remarkably, with the increase of Si content, the water resistance of each catalyst was first enhanced and then weakened. Moreover, all of the wet Si-containing catalysts showed the phenomenon that the benzene conversion decreased in a short time and then followed by a slow recovery. Interestingly, the activities of the silica-containing catalysts exceeded the initial values after the water cut off and did not show a decreasing trend. In brief, the addition of a moderate amount of Si contributed to the enhancement of the water resistance of the Pt_1/CeO_2-based single-atom catalysts, and it also facilitated the improvement of the benzene conversion of the catalysts after the cessation of water vapor. The assistance of non-precious metal Si also proved the enhancement of the water resistance of the catalysts.

In summary, the $Pt_1/CeO_2@SiO_2$-x catalysts have good practical applications in the direction of the study of water resistance. Previously, Hou et al. [30] reported that the generation of hydroxyl-active species would contribute to the enhancement of water resistance of the PdW_1/Al_2O_3 sample. Therefore, we speculated that the silicon-containing catalysts may have generated some hydroxyl-active species at the core-shell interface after water vapor treatment, thus assisting in the enhancement of benzene activity. Additionally, the water resistance of each catalyst was positively correlated with their specific surface areas (Table S2). It may be because the high specific surface area helped in contacting more reactant molecules and water molecules. As a result, the $Pt_1/CeO_2@SiO_2$-x catalysts produced more hydroxyl-active species during contact with water, resulting in favorable catalytic kinetics. Overall, the addition of moderate amounts of silica may favor the production of hydroxyl reactive species, which resulted in excellent water resistance of the $Pt_1/CeO_2@SiO_2$-x samples, and the reactive species was not eliminated after the end of the water and caused an increase in the activities of the catalysts.

3.3. Surface chemical states and redox behaviors of catalysts

Fig. S5a showed the FTIR spectra of the samples before and after water resistance. The peak at 3440 cm^{-1} was attributed to the vibration of physically adsorbed water (H_2O) and surface hydroxyl group (-OH). 1640 cm^{-1} band was related to the vibration of the adsorbed water molecules, and 1570 cm^{-1} belonged to the δ(OH) vibration of H_2O molecules. 1340 cm^{-1} and 1400 cm^{-1} were mainly related to "carbonate-like" substances on the CeO_2 surface by catalyst residues. In addition, a redshift of the Si-O stretching vibration peaks from 1080 cm^{-1} to 1040 cm^{-1} was observed in the $Pt_1/CeO_2@SiO_2$-4 and u-$Pt_1/CeO_2@SiO_2$-4 samples. It suggested that the addition of water may have led to a decrease in the vibrational frequency of the Si-O bond, resulting in a shift of the observed absorption peaks to a lower wavelength [25], which may be related to charge transfer between species.

To investigate the reasons for the remarkable water resistance of the $Pt_1/CeO_2@SiO_2$-x samples and the increase in activity after water treatment, each catalyst was subjected to various characterizations. First, the effect of silicon on the elements was analyzed by the XPS test (Fig. 4). Fig. 4a showed the O spectra of Pt_1/CeO_2 sample were mainly divided into lattice oxygen (O_{latt}) and adsorbed oxygen (O_{ads}). In the $Pt_1/CeO_2@SiO_2$-x samples, the O 1 s spectra were divided into four peaks, 529.3–529.8, 531.4–531.8, 532.2–532.4, and 532.9–533.2 eV, which correspond to the lattice oxygen (O_{latt}), the surface adsorbed oxygen (O_{ads}), the Si-O-Si groups, and the hydroxyl groups (O_{OH}), respectively [31]. The peak of hydroxyl groups was composed of the hydroxyl group of water and silanol (Si-OH). Furthermore, as the thickness of the silicon shell increased, O_{latt} decreased significantly, which indicated that SiO_2 could uniformly cover the surface of the CeO_2 support, resulting in the lattice oxygen on CeO_2 being difficult to detect. However, the O_{latt} on the surface of the $Pt_1/CeO_2@SiO_2$-x sample was relatively abundant when the silicon layer content was 2%, suggesting that SiO_2 was not completely covered on the CeO_2 surface at this time. The ratios of various oxygen species were shown in Table S3. In terms of combined activity (Fig. 3a), O_{latt} could be used as an active species for benzene catalytic combustion. Interestingly, comparing the O spectra (Fig. 4b) of the $Pt_1/CeO_2@SiO_2$-4 catalyst (before adding water) and u-$Pt_1/CeO_2@SiO_2$-4 catalyst (after the addition of water), there was a significant rise in the content of O_{ads} and O_{latt}. It is generally believed that the active species would be slightly reduced after the catalysts participated in the reaction. However, the O_{latt} ratio of the $Pt_1/CeO_2@SiO_2$-4 catalyst increased from 9.48% to 13.59% after the water cut off, which may be related to the water resistance of the catalyst. Therefore, the reason for such a significant increase in catalyst activity after the cessation of water vapor may be related to the nearly 5% increase in O_{ads} content. It may be that the assistance of silicon caused the interactions at the core-shell interface thereby changing the electronic structure, which was consistent with the FTIR result.

In addition, we performed He-TPD experiments (Fig. 4c) on fresh sample ($Pt_1/CeO_2@SiO_2$-4) and water-resistant sample (u-$Pt_1/CeO_2@SiO_2$-4) under He flow, respectively. There were three desorption peaks at 110 °C and 700–800 °C, which were respectively caused by the desorption of the surface-adsorbed hydroxyl species and lattice oxygen species [32,33]. Compared with the fresh sample, the used sample showed significant desorption peaks at 350 °C. The complete elimination temperature of benzene on the $Pt_1/CeO_2@SiO_2$-4 catalyst was at 240 °C, which was much lower than the desorption temperature of the oxygen species. It can be inferred that chemisorbed oxygen species appeared on the surface of the sample after the water resistance test.

In conclusion, the XPS O1s and He-TPD results indicated the generation of more adsorbed oxygen species on the $Pt_1/CeO_2@SiO_2$-4 sample in humid environments, whereas silica-containing catalysts in dry environments, as well as Pt_1/CeO_2 catalyst, were unable to generate such adsorbed oxygen species. In this context, we suggested that water molecules provided surface hydroxyl groups (*OH) through the core-shell interface and played a key role in the oxidation of the reactants with the activation of the active sites [25]. Liu et al. [34] showed that the activation process of oxygen over the $Pt_1/CeO_2@SiO_2$-x catalysts could lead to the generation of new species through hydrogen transfer on the hydroxyl group. Consequently, the incorporation of the silicon layer was beneficial to assisting the participation of H_2O in the catalytic oxidation reaction, which promoted the enhancement of the catalytic activity. Notably, no similar phenomenon occurred over the Pt_1/CeO_2 catalyst, suggesting that these results were inextricably linked to the presence of H_2O.

The Ce 3d spectra (Fig. 4d) could be fitted to eight peaks corresponding to Ce^{4+} species (u′′′, u′′, u, v′′′, v′′, v) and Ce^{3+} species (u′′, v′′) [35], and the ratios of the valence states of Ce element were also summarized in Table S3. Comparing the $Pt_1/CeO_2@SiO_2$-4 catalyst before and after water treatment (Fig. S5b), it can be observed that the ratio of Ce species was not significant, so the effect of Ce species on

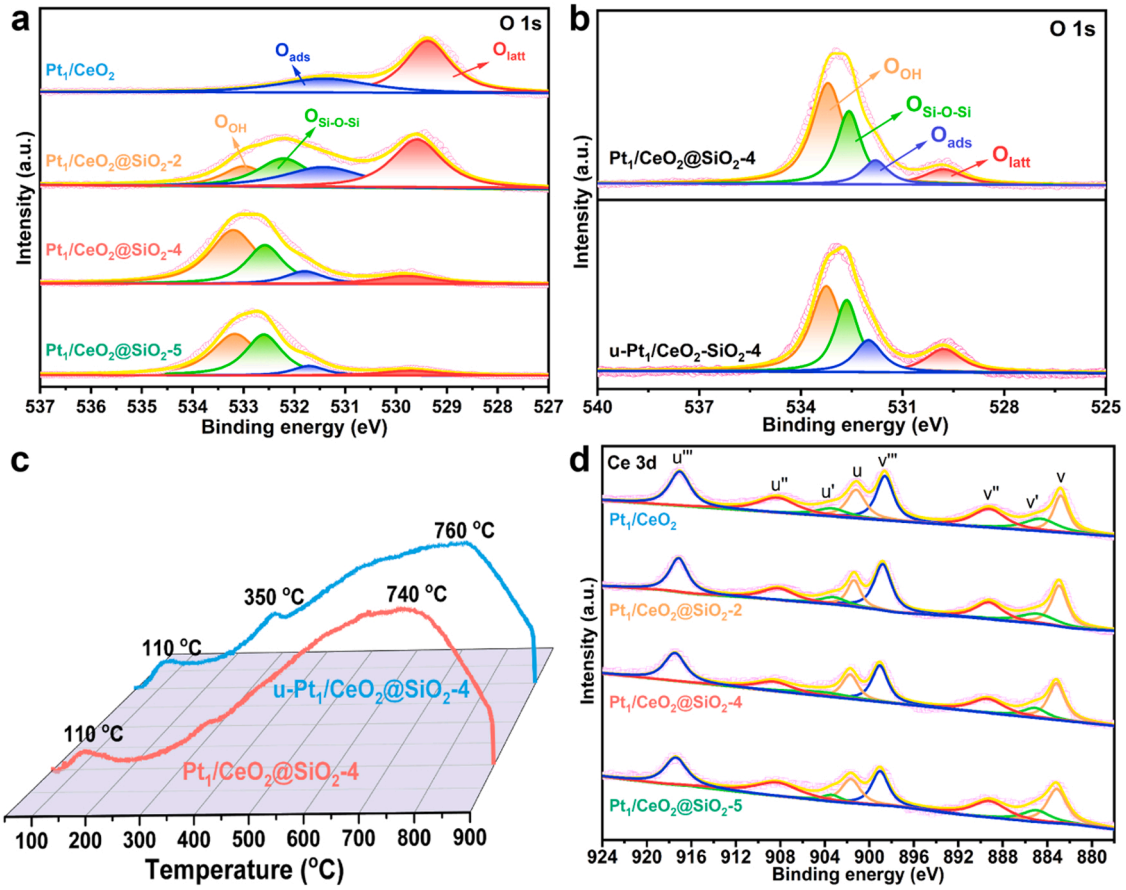

Fig. 4. The O 1 s XPS spectra (a, b), the He-TPD graph (c), and the Ce 3d XPS spectra (d) of the samples.

catalyst activity was not considered. In Fig. S5c, the Pt 4 f spectra showed that the Pt species of the catalysts were mainly Pt ions ($Pt^{\delta+}$) [36], suggesting that the Pt species in the $Pt_1/CeO_2@SiO_2$-4 catalyst were mainly presented in single atoms, which corresponded to the results of XAS and in situ DRIFTS of CO adsorption. Differently, after a long period of operation under water vapor conditions, the content of high valence state ($Pt^{\delta+}$) over the u-$Pt_1/CeO_2@SiO_2$-4 catalyst gradually increased. Consequently, the generation of $Pt^{\delta+}$ species may be one of the reasons for the enhanced performance of the $Pt_1/CeO_2@SiO_2$-4 sample. More importantly, in Table S4, the contents of the Pt surface element on the fresh $Pt_1/CeO_2@SiO_2$-4 and used $Pt_1/CeO_2@SiO_2$-4 catalysts (u-$Pt_1/CeO_2@SiO_2$-4) were 0.06%. In addition, the Pt content on the surface of the fresh Pt_1/CeO_2 catalyst was 0.15%, while it was difficult to detect the Pt content on the surface of the used Pt_1/CeO_2 catalyst. This phenomenon indicated that the Pt species on the surface of the Pt_1/CeO_2 single-atom catalyst migrated and agglomerated significantly after use. Therefore, the addition of the silica shell layer could effectively restrict the active sites and provide a unique chemical environment to avoid the migration and agglomeration phenomena of the noble metals. The core-shell structure could also effectively immobilize and isolate the Pt single atoms during the thermocatalytic reaction process, which also suggested that there was an interaction between the SiO_2 shell and the Pt SAs. We also compared the signal strength of the Ce species, and the XPS spectra in Fig. S5d showed a great difference. Similarly, in conjunction with the Pt 4 f XPS result, the signals of Pt 4 f and Ce 3d spectra weaken with the thickening of the silicon layer. We provided the ratio of each reactive oxygen species in Table 1. It can be found that the O_{latt} and $Pt^{\delta+}$ species were the active species for Pt_1/CeO_2 single-atom catalysts. Moreover, there was a strong connection between O_{ads} and active species as well as the water resistance of silicon-containing catalysts.

Table 1
The XPS data of active oxygen species of catalysts.

Catalysts	O_{latt}/O_{total}	O_{ads}/O_{total}
Pt_1/CeO_2	63.85%	36.15%
$Pt_1/CeO_2@SiO_2$-2	38.10%	25.13%
$Pt_1/CeO_2@SiO_2$-4	9.48%	9.95%
u-$Pt_1/CeO_2@SiO_2$-4	13.59%	14.22%
$Pt_1/CeO_2@SiO_2$-5	7.21%	7.66%

We also explored the redox properties of the samples with the help of the H_2-TPR technique. As shown in Fig. 5a, the H_2-TPR reduction peaks of each sample were closely related to the valence state of the elements, the dispersion state of Pt, the interaction between Pt and CeO_2 support, and the close relationship between Pt, CeO_2, and SiO_2. Pure CeO_2 showed two reduction peaks at 295 °C and 610 °C [37]. The first peak was mainly related to the reduction of Ce^{4+} species over CeO_2 and the reduction of surface oxygen species. The second reduction peak belonged to the reduction of Ce^{4+} to Ce^{3+} species and the reduction of lattice oxygen within CeO_2 [38]. Therefore, compared to pure CeO_2, the peaks on the Pt_1/CeO_2 sample were all in the lower temperature range, and the reduction peak at 95 °C was related to the reduction of Pt species. This phenomenon suggested that the addition of Pt species effectively reduced the reduction temperature of CeO_2, and it revealed the possible presence of Pt-CeO_2 interaction on the sample surface, which was also consistent with the EXAFS result [39]. The reduction peak at 154 °C over the $Pt_1/CeO_2@SiO_2$-2 sample was also thought to be related to the reduction of Pt species. However, the incorporation of the silicon layer may affect the movement of the Pt reduction peak toward higher temperatures. In addition, the reduction peaks at 250–450 °C were attributed to the reduction of large amounts of CeO_2 surface oxygen

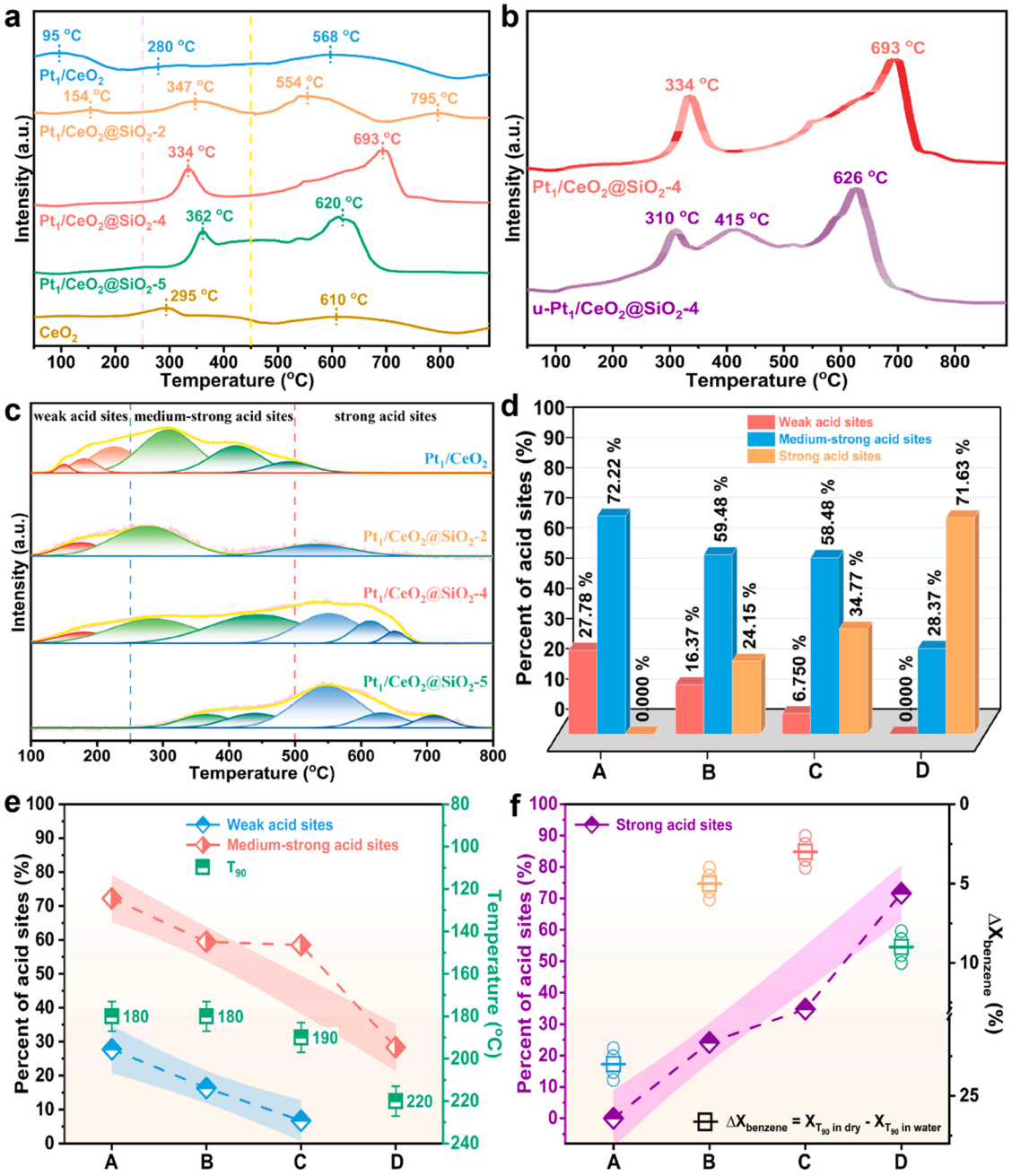

Fig. 5. H_2-TPR curves (a, b) and NH_3-TPD curves (c). The percentage of each acid site (d), the relationship between T_{90} and acid site ratios (e), and the relationship between $\Delta X_{benzene}$ and the strong acid sites ratio (f) of Pt_1/CeO_2 (A), $Pt_1/CeO_2@SiO_2$-2 (B), $Pt_1/CeO_2@SiO_2$-4 (C), $Pt_1/CeO_2@SiO_2$-5 (D) samples.

species and Ce^{4+} species, while the peaks above 450 °C were generally considered to be the reduction of lattice oxygen within CeO_2. In general, H_2 molecules are preferentially activated at the Pt active sites, whereby active hydrogen overflows to the CeO_2 surface. The low Pt content and the Pt-O-Ce interactions allowed some of the CeO_2 located at the interface to be reduced at lower temperatures. Combined with the O 1 s XPS spectra (Fig. 4a), the Pt_1/CeO_2 sample contained more surface lattice oxygen than the $Pt_1/CeO_2@SiO_2$-2 sample, so the reduction peaks appearing in the temperature below 250 °C may also be related to the reduction of the surface oxygen of CeO_2.

To deeply investigate the relationship between the redox properties and water resistance of the samples, we performed H_2-TPR on the samples with high Si content, and the results were shown in Fig. 5a. With the increase of silicon content, the $Pt_1/CeO_2@SiO_2$-4 sample and the $Pt_1/CeO_2@SiO_2$-5 sample did not show significant reduction peaks at low temperatures (<250 °C). After the introduction of SiO_2 on the CeO_2 surface, the Si-containing samples showed obvious hydrogen absorption peaks, confirming the existence of a certain degree of interaction between the core layer (Pt-CeO_2) and the SiO_2 shell layer. Moreover, the reduction peaks located in the temperature band of 250–450 °C slowly moved towards higher temperatures with the increase of silicon content. Among them, the reduction peak of the $Pt_1/CeO_2@SiO_2$-4 sample had the weakest trend to move, indicating the easier reduction of CeO_2 on the $Pt_1/CeO_2@SiO_2$-4 sample compared to other Si-containing samples. Furthermore, through the specific surface area of the samples (Table S2), the sample with a large specific surface area indicated a more uniform dispersion of CeO_2 nanoparticles per unit area. As a result, the small particles of CeO_2 dispersed on the surface of the $Pt_1/CeO_2@SiO_2$-4 sample come into contact with more H_2 molecules compared to the other Si-containing samples, which caused the reduction peak of CeO_2 on the

surface to move to lower temperatures. Similarly, in the temperature section above 450 °C, each reduction peak shifted to higher reduction temperatures with increasing silicon content, which may be related to the production of Ce-Si solid composite oxides with higher reduction temperatures [40]. Interestingly, the $Pt_1/CeO_2@SiO_2$-2 sample showed two distinct reduction peaks at 554 °C and 795 °C, which may be related to the inhomogeneous coverage of the SiO_2 layer. This suggested that there was bare CeO_2 on the catalyst surface, and H_2 molecules were more likely to aggregate on the bare CeO_2, making the lattice oxygen within CeO_2 more easily reduced. We also tested the H_2-TPR of the $Pt_1/CeO_2@SiO_2$-4 sample after water resistance (u- $Pt_1/CeO_2@SiO_2$-4). From the curves (Fig. 5b), it can be noticed that compared to the fresh $Pt_1/CeO_2@SiO_2$-4 sample, the reduction peaks of the u-$Pt_1/CeO_2@SiO_2$-4 sample were all moved towards lower temperatures. Moreover, a new reduction peak appeared at 415 °C, which may be attributed to the reduction of the generated adsorbed oxygen species after water resistance. This comparison revealed that the reducing performance of Ce species and O species on the surface of the u-$Pt_1/CeO_2@SiO_2$-4 sample was enhanced during the activation of H_2 molecules, and it was speculated that it might be related to the formation of oxygen species.

For insight into the water resistance of $Pt_1/CeO_2@SiO_2$-x, O_2-TPD tests were performed for each catalyst to observe the migration of oxygen species (Fig. S6). The peaks of oxygen species were three types [41]: desorption of surface adsorbed oxygen species at 100–300 °C, desorption of surface lattice oxygen at 300–500 °C, and detachment of bulk lattice oxygen (>500 °C). In Fig. S6a, the silicon-containing catalysts exhibited richer oxygen species, indicating that the addition of the silica layer accelerated the migration of some lattice oxygen species, which laterally confirmed the existence of certain interactions between the Pt-CeO_2 core and the SiO_2 shell. Moreover, the migration of partial lattice oxygen may be one of the reasons for the enhancement of water resistance of the catalysts. In the benzene combustion process, the surface acid has an important effect on the adsorption of reactants. The NH_3-TPD method could determine the surface acid of each sample, as shown in Fig. 5c. It is generally accepted that the peaks at 100–250 °C were attributed to weak acid sites, the desorption peaks at 250–500 °C corresponded to medium strong acid sites, and the peaks at 500–800 °C were classified as strong acid sites [42]. The percentages of each acid site were also summarized in Table 2. From Fig. 5d, the percentage of weak acid sites gradually decreased and the percentage of strong acid sites increased with the thickening of the SiO_2 shell layer. Combined with the activity, more weak and medium strong acid sites favored for the adsorption of benzene molecules (Fig. 5e). The water resistance of the $Pt_1/CeO_2@SiO_2$-x samples was significantly improved relative to that of the Pt_1/CeO_2 sample, which might be due to the enhancement of the strong acid sites. As shown in Fig. S6b, we calculated the difference (ΔX) between the benzene conversion of the catalysts in dry air and wet air during the hydrothermal stability test (Fig. S4). The $Pt_1/CeO_2@SiO_2$-x samples showed the most excellent water resistance with the ΔX of 3%. Therefore, we summarized the graph of ΔX versus the ratio of strong acid sites (Fig. 5f), suggesting that the strong acid sites indeed contributed to the water resistance of the silica-containing catalysts. Of course, the proportion of strong acid sites was not the more the better, and excessive strong acid sites would cause the water resistance of the samples to show a decreasing trend. Interestingly, comparing the $Pt_1/CeO_2@SiO_2$-4 sample after water resistance (u-$Pt_1/CeO_2@SiO_2$-4 sample), it can be found that there was a significant increase in the proportion of medium-strong acid sites and a decrease in the ratio of strong acid sites in the u-$Pt_1/CeO_2@SiO_2$-4 sample (Fig. S6c, d). It was hypothesized that the strong acid sites (*OH) on the surface of the catalysts reacted with O_2 and produced oxygen species in the form of medium-strong acid sites when the water was passage. In addition, the surface of the SiO_2 sample contained lots of weak acid sites. When the SiO_2 layer was added, the content of weak acid sites of the $Pt_1/CeO_2@SiO_2$-x samples was significantly weakened, which confirmed the existence of interactions between the core (Pt_1/CeO_2) and the SiO_2 shell layer. The results corresponded to the H_2-TPR result. All in all, we speculated that the moderate amount of strong acid sites and the migration of oxygen species may be one of the reasons for fueling the enhanced water resistance of the Si-catalysts.

Table 2
The Percentage of acid sites of catalysts.

Catalysts	Weak acid sites	Medium-strong acid sites	Strong acid sites
Pt_1/CeO_2	27.78%	72.22%	-
$Pt_1/CeO_2@SiO_2$-2	16.37%	59.48%	24.15%
$Pt_1/CeO_2@SiO_2$-4	6.75%	58.48%	34.77%
u-$Pt_1/CeO_2@SiO_2$-4	10.86%	65.54%	23.60%
$Pt_1/CeO_2@SiO_2$-5	-	28.37%	71.63%

3.4. The investigation of the action of water molecules

An in situ DRIFTS experiment was used for $Pt_1/CeO_2@SiO_2$-4 to investigate the reaction pathway of the benzene combustion process. Fig. 6a, b showed the in situ DRIFTS spectra of the catalyst adsorbing benzene in benzene/N_2 gas at different times. The strong absorption peak at 1638 cm^{-1} was the C═O stretching vibration region, and there may be overlapping peaks of various compounds with carbonyl groups. The weak absorption peaks at 1250–1000 cm^{-1} were mainly related to the characteristic peaks of the C-O species. Moreover, the hydroxyl peaks were gradually enhanced with time, which combined with the above phenomena indicated that benzene may be oxidized to phenolates, benzoquinones, maleates, and even acetate species. It is noteworthy that intermediates were produced during the adsorption process of benzene, indicating that lattice oxygen participated in the activation of benzene at low temperatures to promote the reaction. Fig. 6c revealed that an increase in temperature promoted the generation of phenol (1258 cm^{-1}), and maleate (1454 cm^{-1}). The band at 1570 cm^{-1} was the overlapping peak of the C═C stretching vibration of the phenolates [40] and the COO^- species vibration of maleates or carboxylates [43]. The strong wave at 1625 cm^{-1} was attributed to the carbonyl groups. In addition, the wavebands at 2940 cm^{-1} and 2860 cm^{-1} were mainly associated with C-H bond stretching vibrations [44]. Phenol, benzoquinone, and maleate were hypothesized to be the major intermediates of the $Pt_1/CeO_2@SiO_2$-4 catalyst. The conversion of phenol to intermediates such as benzoquinone or maleate may be one of the key factors in the oxidation process of benzene. The Pt_1/CeO_2 catalyst was also subjected to in situ DRIFTS experiment as a comparison sample, as shown in Figs. S7 and 5d. The absorption peaks of benzoquinone were predominantly present over the Pt_1/CeO_2 catalyst in Fig. S7. The weak band at 1778 cm^{-1} belonged to the characteristic peaks of o-benzoquinone, and the characteristic peak at 1675 cm^{-1} was attributed to p-benzoquinone, which was associated with the C═O stretching vibration [45]. The C═C stretching vibrations of the aromatic ring were mainly located in the range of 1600–1470 cm^{-1}. It is also evident from Fig. 6d that intermediates such as benzoquinone (1660 cm^{-1}) and maleic acid (1456 cm^{-1}, 1530 cm^{-1}, double peaks at 1840–1720 cm^{-1}) gradually accumulated with increasing temperatures [46]. Interestingly, no distinct peak for acetate species was found, suggesting that the benzoquinone and maleic acid intermediates over the Pt_1/CeO_2 catalyst could be directly converted to the final products (CO_2 and H_2O). It turned out that there were different decisive steps on the $Pt_1/CeO_2@SiO_2$-4 and Pt_1/CeO_2 catalysts, which may be related to the addition of silicon shells. In general, the reaction route of benzene followed: benzene → phenol → benzoquinone → maleic acid → CO_2 and H_2O. The addition of silicon made the conversion of benzene with acetate as an additional intermediate product.

According to Fig. S4, the water resistance of the silica-assisted single-atom catalysts was significantly improved, so to clarify the reaction mechanism of the $Pt_1/CeO_2@SiO_2$-4 catalyst in the water-resistant

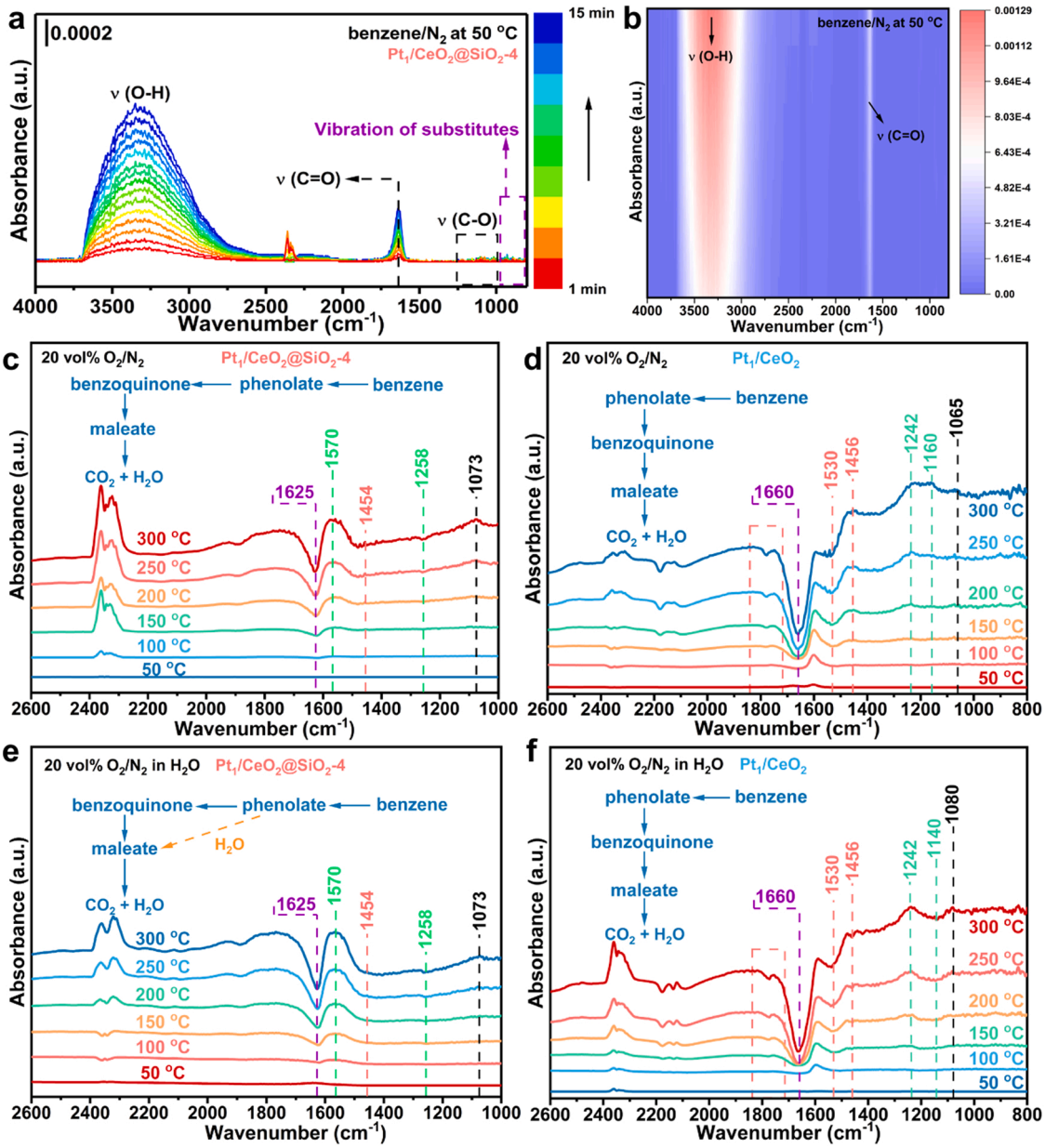

Fig. 6. In situ DRIFTS spectra of benzene adsorption of $Pt_1/CeO_2@SiO_2$-4 catalyst at 50 °C for different times at pure N_2 gas flow (a, b). The in situ DRIFTS spectra of $Pt_1/CeO_2@SiO_2$-4 catalyst (c) and Pt_1/CeO_2 catalyst (d) for different reaction temperatures with the benzene/air gas. The in situ DRIFTS spectra of $Pt_1/CeO_2@SiO_2$-4 catalyst (e) and Pt_1/CeO_2 catalyst (f) for different reaction temperatures in the benzene/air gas with H_2O.

process, we also carried out in-situ DRIFTS experiment under aqueous condition. From Fig. 6e, the benzene activation route was basically the same in O_2/N_2 gas with H_2O as it was in O_2/N_2 gas. Curiously, the introduction of water resulted in a change in the hydroxyl peaks, probably because water was involved in the conversion of benzene during the warming process, which shifted the hydroxyl peak (Fig. S8a), and there was no analogous situation of hydroxyl displacement (Fig. S8b). Based on the activity after water resistance, the introduction of water did contribute to the catalytic decomposition of benzene. Hence, the role of H_2O in the reaction process was explored by performing in situ DRIFTS test at lower temperatures for different times, and the results were shown in Fig. S8c-f. The band at 1665 cm^{-1} was the characteristic peak of benzoquinone at 50 °C in Fig. S8c and there was no strong peak in the 1700–1500 cm^{-1} band. In contrast, a strong band located at 1640 cm^{-1} appeared in Fig. S8d, which was related to the C═O vibrations of benzoquinone, and maleate species. Besides, the characteristic peaks at 2940 cm^{-1} and 2860 cm^{-1} appeared, suggesting that water facilitated the decomposition of benzene at 50 °C. The spectrum showed a strong peak of maleate (1548 cm^{-1}) at 100 °C in Fig. S8e. The distinct characteristic peak of phenol (1570 cm^{-1}) appeared at 100 °C in Fig. S8f, confirming that the introduction of water could reduce the production of benzoquinone so that the phenol could directly produce intermediates such as maleate species, which accelerated the catalytic reaction of benzene and shortened the reaction pathway. Likewise, the Pt_1/CeO_2 comparative sample was also performed as an in situ DRIFTS test under the water atmosphere. The conversion of benzene over the Pt_1/CeO_2 catalyst was not significantly impacted by water (Fig. 6f). As seen in Fig. S9, the intensities of the peaks of the Pt_1/CeO_2 catalyst under anhydrous conditions were significantly higher than those of the wave peaks under aqueous conditions. Interestingly, at low temperatures, the $Pt_1/CeO_2@SiO_2$-x and Pt_1/CeO_2 catalysts showed opposite phenomena under dry and wet conditions, suggesting that water over the $Pt_1/CeO_2@SiO_2$-x catalysts facilitated the activation of benzene, while water over the Pt_1/CeO_2

catalysts inhibited the catalytic oxidation process of benzene due to the adsorption of water molecules at the active sites.

To clarify the structure of oxygen species occurring, the in situ DRIFTS spectra in the range of 1500–600 cm^{-1} were analyzed in detail at 50 °C (Fig. 7a). New vibrational bands appeared at 1220–1030 cm^{-1}, 840 cm^{-1}, and 960–730 cm^{-1} in the plots after the introduction of water vapor [47]. On the surface of the $Pt_1/CeO_2@SiO_2$-4 sample, silica assisted the reaction of O_2 with H_2O and generated hydroperoxyl (*OOH) which may be the key factor for the good water resistance of the $Pt_1/CeO_2@SiO_2$-x catalysts and the increase in activity after the water cut off. Therefore, the vibrational peaks of hydroxyl species at $\delta_{OO\text{-}H}$ and $\nu_{O\text{-}O}$ were attributed to 1220–1030 cm^{-1} and 840 cm^{-1}, respectively [48]. The band at 960–730 cm^{-1} was mainly the overlapping band of $\nu_{O\text{-}O}$ peaks of the metal peroxide complexes and the metal superoxide complexes. Nevertheless, in the absence of water conditions, these absorption peaks did not exist on the surface of the $Pt_1/CeO_2@SiO_2$-4 sample. As reported in the literature [29], O_2 was protonated with H_2O, resulting in the formation of hydroperoxyl (*OOH). So, the new species produced on the surface of the $Pt_1/CeO_2@SiO_2$-4 sample was hydroperoxide species. In addition, the vibrational and rotational bands of water at 1460 cm^{-1} indicated that the Pt_1/CeO_2 surface was prone to adsorb water molecules. During the water passage process, water and reactants had competitive adsorption on the surface of the Pt_1/CeO_2 catalyst, thus decreasing the water resistance. Moreover, the presence of the silicon layer helped to isolate the direct contact of water with the active sites and promoted the water resistance of the silicon-containing catalysts.

4. Discussion

Typically, the adsorption, dissociation, and desorption of reactants and water molecules on the surface of catalysts were related to the electronic structure of the active sites [49]. According to the EXAFS, in situ DRIFTS of CO adsorption and XPS results, Pt single atoms mainly existed in the $Pt_1/CeO_2@SiO_2$-4 catalyst and no agglomeration of Pt SAs occurred after the reaction, indicating that the $Pt_1/CeO_2@SiO_2$-x samples anchored the Pt SAs with the help of CeO_2 support while utilizing the SiO_2 layer for immobilization during the thermocatalytic process, which revealed a close relationship between Pt, CeO_2 and SiO_2. Combining the performance of the catalysts and the XPS results, we believe that the electronic structure of the core-shell interface changed under the interaction between the SiO_2 shell layer and the Pt-CeO_2 core layer. We also further confirmed the interaction between Pt, CeO_2 and SiO_2 by the H_2-TPR technique. In addition, the formation of oxygen-rich species and the change of weak acid sites also confirmed the interaction between the core and shell layers of the Si-containing catalysts. Combined with Figs. S3 and 6a, the in situ DRIFTS technique was used to elucidate the formation and structure of reactive oxygen species in Si-containing catalysts in the presence of water, and the presence of reactive species effectively contributed to the enhancement of benzene activity. Therefore, based on the performance and XPS results of the catalysts, we assumed that the electronic structure of the core-shell interface changed with the assistance of the silica layer and water molecules, which led to the creation of an active interface and participated in the activation of the hydroxyl species (*OH) and O_2 to generate new oxygen species. This phenomenon was comparable to what Hou et al. reported [29]. The H_2-TPR result (Fig. 5b) also confirmed the

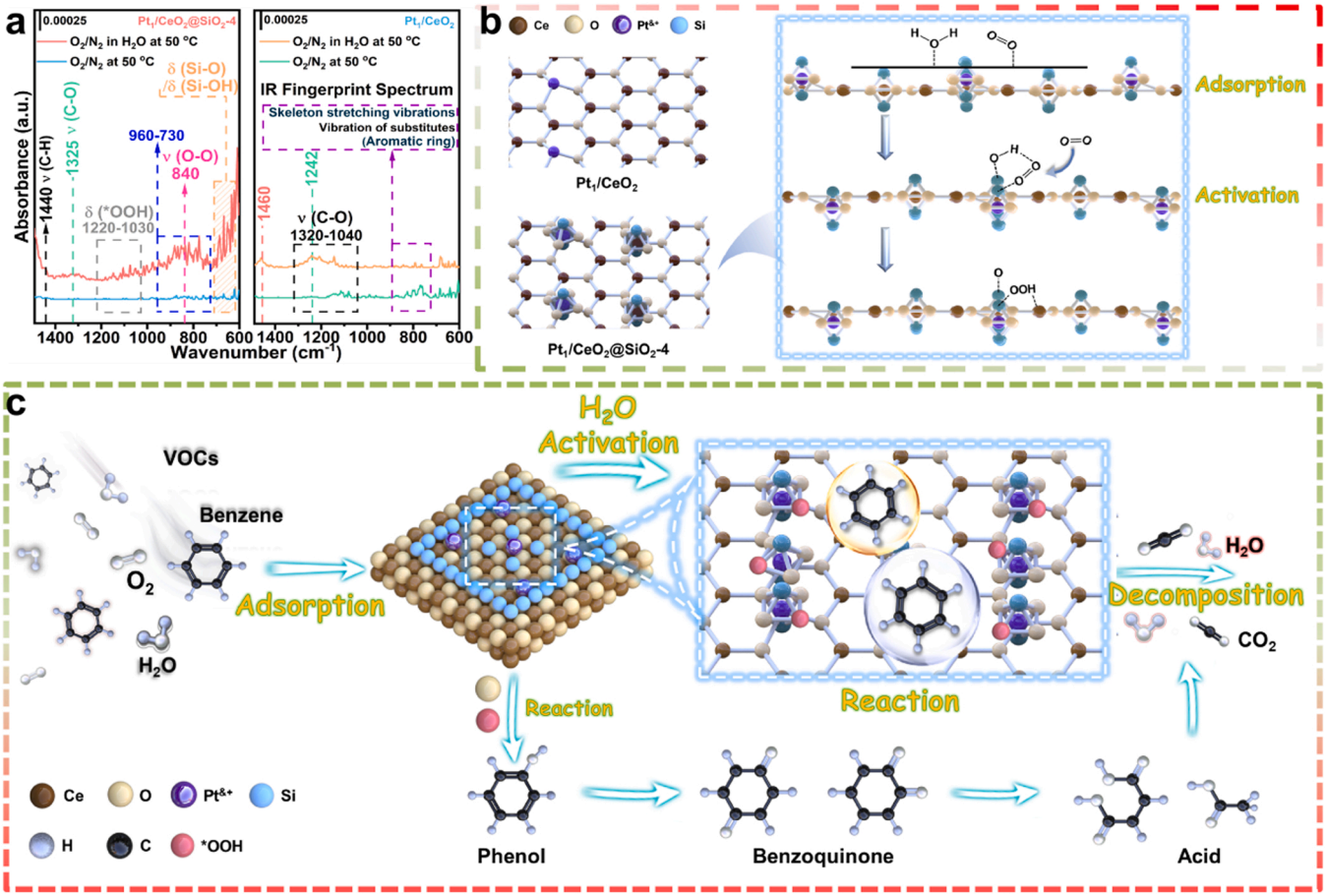

Fig. 7. In situ DRIFTS spectra of $Pt_1/CeO_2@SiO_2$-4 and Pt_1/CeO_2 catalysts in the 1500–600 cm^{-1} band (a). The oxygen activation pathway on the $Pt_1/CeO_2@SiO_2$ catalysts (b) and the reaction mechanism diagram of $Pt_1/CeO_2@SiO_2$ catalyst under a humid environment (c).

presence of reactive oxygen species (*OOH) under the aqueous condition. All in all, in the humid environment, the generation of new reactive oxygen species may undergo charge transfer with the active species, thus promoting the growth of active species, thus contributing to the catalytic combustion of benzene over the $Pt_1/CeO_2@SiO_2$-x catalysts.

Furthermore, correlating the conclusion of He-TPD and NH_3-TPD, the silica layer of the $Pt_1/CeO_2@SiO_2$-x samples assisted in the generation of new reactive adsorbed oxygen (*OOH) species. It revealed that the strong acid sites might enhance the dissociation of water molecules in the SiO_2 layer and generate hydroxyl species, thus fueling the formation of the Pt-O-Si active interface. Apparently, the catalytic combustion process of benzene was strongly associated with each acid site in the humid environment. On the one hand, weak acid sites and medium-strong acid sites would drive the conversion of benzene. On the other hand, an appropriate amount of strong acid sites in contact with water molecules may improve the charge distribution at the core-shell interface, thus promoting the activation of H_2O and O_2 to generate reactive oxygen species (*OOH). In sum, the strong acid sites might alter the contact way of water molecules in wet air, thus diminishing the competitive adsorption of H_2O with the reactants.

To summarize, we hypothesized a new pathway for oxygen activation to occur at the Pt-O-Si active interface of the catalyst when containing water: Si-OH + O_2 → *OOH + *O-Si. We also proposed a diagram of the oxygen activation pathway applicable to the Pt-O-Si active interface, as shown in Fig. 7b. When water was added, the surface of the Si layer was prone to promote the adsorption of hydroxyl species, changing the local electronic structure. The strong interaction of Pt-CeO_2 also induced electron transfer. The combined effect of the above two parts led to the creation of Pt-O-Si active interfaces at the core-shell interfaces. In sum, H_2O and adsorbed O_2 protonated at the Pt-O-Si active interface [50] and accelerated the oxidation of benzene, which served as a driving force for the enhancement of the catalyst's water resistance. The introduction of the SiO_2 coating not only facilitated the adsorption and dissociation of intermediates but also changed the reaction pathway of benzene conversion. According to the in situ DRIFTS results, we proposed a feasible reaction pathway for benzene combustion on the surface of $Pt_1/CeO_2@SiO_2$-4 catalyst (Fig. 7c). As the catalyst could show intermediates during adsorption, it indicated that the lattice oxygen within the catalyst would participate in the benzene oxidation process. Therefore, we believed that benzene catalytic combustion over $Pt_1/CeO_2@SiO_2$-4 catalyst was realized through the joint action of MvK and L-H mechanisms, and the L-H mechanism was mainly dominated in the water-resistant process. Most importantly, the addition of water promoted the activation of oxygen species at the Pt-O-Si interface. After the water cut off, the water on the surface of the Pt_1/CeO_2 catalyst would leave, while the *OOH species as new reactive oxygen species on the surface of the $Pt_1/CeO_2@SiO_2$-4 catalyst remained to improve its catalytic performance.

In conclusion, the shielding effect of the silica layer, not only prevented the sintering of Pt single atoms but also attenuated the direct contact of water molecules with the active sites, thus effectively inhibiting the occurrence of competitive adsorption. On the $Pt_1/CeO_2@SiO_2$-4 SAC, water molecules in contact with the silica layer formed hydroxyl species and caused changes in the local structure of the catalyst core-shell. Moreover, the strong Pt-CeO_2 interaction also promoted the charge transfer at the core-shell interface, which facilitated the generation of Pt-O-Si active interface and reactive oxygen species (*OOH) which effectively contributed to the water resistance of the $Pt_1/CeO_2@SiO_2$-4 catalyst. Moreover, the strong acid sites on the surface were also favorable for promoting the water resistance of the $Pt_1/CeO_2@SiO_2$-4 catalyst. In short, the changes in the local electronic structure of the core-shell interface fueled the protonation of H_2O and O_2 to generate new reactive oxygen (*OOH) species. It not only effectively promoted the water resistance of $Pt_1/CeO_2@SiO_2$-x catalysts, but also supported the enhancement of the performance of silicon-containing catalysts.

5. Conclusion

In conclusion, we have successfully designed a Pt single-atom catalyst with excellent activity. Moreover, the addition of a silica layer improved the water resistance of the Pt single-atom catalyst while maintaining the good activity of the $Pt_1/CeO_2@SiO_2$-4 catalyst. Various characterization techniques showed that the shielding effect of the silica layer not only prevented the sintering of Pt single atoms but also avoided the direct contact of water molecules with the active sites, which effectively improved the water resistance of the single-atom catalyst. In situ DRIFTS and TPD experiments jointly confirmed the specific role of water in benzene catalytic combustion. The results showed that in humid environments, the introduction of the silica layer could construct a Pt-O-Si active interface, which assisted in the activation of O_2 and H_2O. It promoted the generation of new reactive oxygen species (*OOH) and resulted in the enhancement of the water resistance ability of the $Pt_1/CeO_2@SiO_2$ catalysts. This finding contributed to an in-depth understanding of the effect of water on the catalytic oxidation of VOCs and provided a direction of thinking for the rational design of single-atom catalysts with strong water resistance.

Declaration of Competing Interest

The authors declare that they have no known competing financial interests or personal relationships that could have appeared to influence the work reported in this paper.

Data Availability

The authors do not have permission to share data.

Acknowledgments

This work was supported by the National Natural Science Foundation of China (52070182), Province Natural Science Foundation of GanSu (23JRRA638, 23JRRA622), Talents of Innovation and Entrepreneurship Project of Lanzhou, China (2022-RC-26), West Light Foundation of the Chinese Academy of Sciences (xbzg-zdsys-202318), Science and Technology Program of Lanzhou City (2023-3-35), the Key Research and Development Program of Gansu Province (23YFFA0012).

Appendix A. Supporting information

Supplementary data associated with this article can be found in the online version at doi:10.1016/j.apcatb.2024.124152.

References

[1] S.C. Kim, W.G. Shim, Catalytic combustion of VOCs over a series of manganese oxide catalysts, Appl. Catal. B: Environ. 98 (2010) 180–185.
[2] S. Zhao, F. Hu, J. Li, Hierarchical Core–Shell Al_2O_3@Pd-CoAlO Microspheres for Low-Temperature Toluene Combustion, ACS Catal. 6 (2016) 3433–3441.
[3] X.F. Yang, A. Wang, B. Qiao, J. Li, J. Liu, T. Zhang, Single-atom catalysts: a new frontier in heterogeneous catalysis, Acc. Chem. Res. 46 (2013) 1740–1748.
[4] X.F. Cheng, J.H. He, H.Q. Ji, H.Y. Zhang, Q. Cao, W.J. Sun, C.L. Yan, J.M. Lu, Coordination symmetry breaking of single-atom catalysts for robust and efficient nitrate electroreduction to ammonia, Adv. Mater. 34 (2022) e2205767.
[5] W. Li, Z. Guo, J. Yang, Y. Li, X. Sun, H. He, S. Li, J. Zhang, Advanced strategies for stabilizing single-atom catalysts for energy storage and conversion, Electrochem. Energy R. 5 (2022) 9.
[6] J. Shan, C. Ye, Y. Jiang, M. Jaroniec, Y. Zheng, S.Z. Qiao, Metal-metal interactions in correlated single-atom catalysts, Sci. Adv. 8 (2022) eabo0762.
[7] J. Shan, C. Ye, C. Zhu, J. Dong, W. Xu, L. Chen, Y. Jiao, Y. Jiang, L. Song, Y. Zhang, M. Jaroniec, Y. Zhu, Y. Zheng, S.Z. Qiao, Integrating interactive noble metal single-atom catalysts into transition metal oxide lattices, J. Am. Chem. Soc. 144 (2022) 23214–23222.
[8] Y. Zhang, J. Yang, R. Ge, J. Zhang, J.M. Cairney, Y. Li, M. Zhu, S. Li, W. Li, The effect of coordination environment on the activity and selectivity of single-atom catalysts, Coord. Chem. Rev. 461 (2022) 214493.

[9] Y. Shen, J. Deng, X. Hu, X. Chen, H. Yang, D. Cheng, D. Zhang, Expediting toluene combustion by harmonizing the Ce–O strength over Co-doped CeZr oxide catalysts, Environ. Sci. Technol. 57 (2023) 1797–1806.

[10] X.-F. Wang, C.-F. Liu, L.-C. He, B. Li, J.-Q. Lu, M.-F. Luo, J. Chen, Unveiling geometric and electronic effects of Pt species on water-tolerant Pt/ZSM-5 catalyst for propane oxidation, Appl. Catal. A: Gen. 655 (2023) 119108.

[11] Y. Shen, J. Deng, S. Impeng, S. Li, T. Yan, J. Zhang, L. Shi, D. Zhang, Boosting toluene combustion by engineering Co–O strength in cobalt oxide catalysts, Environ. Sci. Technol. 54 (2020) 10342–10350.

[12] X.-F. Wang, L.-Y. Xu, C.-H. Wen, D.-D. Li, B. Li, J.-Q. Lu, Q.-H. Yang, M.-F. Luo, J. Chen, WO_3 boosted water tolerance of Pt nanoparticle on SO_4^{2-}-ZrO_2 for propane oxidation, Appl. Catal. B: Environ. 338 (2023) 123000.

[13] S. Zhao, Y. Wen, X. Liu, X. Pen, F. Lü, F. Gao, X. Xie, C. Du, H. Yi, D. Kang, X. Tang, Formation of active oxygen species on single-atom Pt catalyst and promoted catalytic oxidation of toluene, Nano Res 13 (2020) 1544–1551.

[14] Y. Ji, S. Liu, S. Song, W. Xu, L. Li, Y. Zhang, W. Chen, H. Li, J. Jiang, T. Zhu, Z. Li, Z. Zhong, D. Wang, G. Xu, F. Su, Negatively charged single-atom Pt catalyst shows superior SO_2 tolerance in NO_x reduction by CO, ACS Catal. 13 (2022) 224–236.

[15] M. Xiao, D. Han, X. Yang, N. Tsona Tchinda, L. Du, Y. Guo, Y. Wei, X. Yu, M. Ge, Ni-doping-induced oxygen vacancy in Pt-CeO_2 catalyst for toluene oxidation: Enhanced catalytic activity, water-resistance, and SO_2-tolerance, Appl. Catal. B: Environ. 323 (2023) 122173.

[16] C. Wang, X.-K. Gu, H. Yan, Y. Lin, J. Li, D. Liu, W.-X. Li, J. Lu, Water-mediated Mars-Van Krevelen mechanism for CO oxidation on ceria-supported single-atom Pt_1 catalyst, ACS Catal. 7 (2016) 887–891.

[17] W.H. Li, J. Yang, H. Jing, J. Zhang, Y. Wang, J. Li, J. Zhao, D. Wang, Y. Li, Creating high regioselectivity by electronic metal-support interaction of a single-atomic-site catalyst, J. Am. Chem. Soc. 143 (2021) 15453–15461.

[18] S. Chen, W.H. Li, W. Jiang, J. Yang, J. Zhu, L. Wang, H. Ou, Z. Zhuang, M. Chen, X. Sun, MOF encapsulating N-heterocyclic carbine-ligated copper single-atom site catalyst towards efficient methane electrosynthesis, Angew. Chem. Int. Ed. 134 (2022) e202114450.

[19] J. Yang, W.H. Li, S. Tan, K. Xu, Y. Wang, D. Wang, Y. Li, The electronic metal–support interaction directing the design of single atomic site catalysts: achieving high efficiency towards hydrogen evolution, Angew. Chem. Int. Ed. 133 (2021) 19233–19239.

[20] J.H. Kim, D. Shin, J. Lee, D.S. Baek, T.J. Shin, Y.T. Kim, H.Y. Jeong, J.H. Kwak, H. Kim, S.H. Joo, A general strategy to atomically dispersed precious metal catalysts for unravelling their catalytic trends for oxygen reduction reaction, ACS Nano 14 (2020) 1990–2001.

[21] H. Peng, C. Rao, N. Zhang, X. Wang, W. Liu, W. Mao, L. Han, P. Zhang, S. Dai, Confined ultrathin Pd-Ce nanowires with outstanding moisture and SO_2 tolerance in methane combustion, Angew. Chem. Int. Ed. 57 (2018) 8953–8957.

[22] J. Zhang, X. Qin, X. Chu, M. Chen, X. Chen, J. Chen, H. He, C. Zhang, Tuning metal–support interaction of Pt-CeO_2 catalysts for enhanced oxidation reactivity, Environ. Sci. Technol. 55 (2021) 16687–16698.

[23] J. Liu, L. Wang, F. Okejiri, J. Luo, J. Zhao, P. Zhang, M. Liu, S. Yang, Z. Zhang, W. Song, W. Zhu, J. Liu, Z. Zhao, G. Feng, C. Xu, S. Dai, Deep understanding of strong metal interface confinement: a journey of Pd/FeO_x catalysts, ACS Catal. 10 (2020) 8950–8959.

[24] T. Pu, W. Zhang, M. Zhu, Engineering heterogeneous catalysis with strong metal-support interactions: characterization, theory and manipulation, Angew. Chem. Int. Ed. 62 (2023) e202212278.

[25] T. Dong, J. Ji, L. Yu, P. Huang, Y. Li, Z. Suo, B. Liu, Z. Hu, H. Huang, Tunable interfacial electronic Pd-Si interaction boosts catalysis via accelerating O_2 and H_2O activation, JACS Au 3 (2023) 1230–1240.

[26] H. Jeong, D. Shin, B.S. Kim, J. Bae, S. Shin, C. Choe, J.W. Han, H. Lee, Controlling the oxidation state of Pt single atoms for maximizing catalytic activity, Angew. Chem. Int. Ed. 59 (2020) 20691–20696.

[27] W. Tan, S. Xie, Y. Cai, M. Wang, S. Yu, K.-B. Low, Y. Li, L. Ma, S.N. Ehrlich, F. Gao, L. Dong, F. Liu, Transformation of highly stable Pt single sites on defect engineered ceria into robust Pt clusters for vehicle emission control, Environ. Sci. Technol. 55 (2021) 12607–12618.

[28] H. Shi, H. Wang, Y. Zhou, J. Li, P. Zhai, X. Li, G.G. Gurzadyan, J. Hou, H. Yang, X. Guo, Atomically dispersed indium-copper dual-metal active sites promoting C−C coupling for CO_2 photoreduction to ethanol, Angew. Chem. Int. Ed. 61 (2022) e202208904.

[29] F. Dong, Y. Meng, W. Ling, W. Han, W. Han, X. Li, Z. Tang, Single atomic Pt confined into lattice defect sites for low-temperature catalytic oxidation of VOCs, Appl. Catal. B: Environ. Energy 346 (2024) 123779.

[30] Z. Hou, L. Dai, J. Deng, G. Zhao, L. Jing, Y. Wang, X. Yu, R. Gao, X. Tian, H. Dai, D. Wang, Y. Liu, Electronically engineering water resistance in methane combustion with an atomically dispersed tungsten on PdO catalyst, Angew. Chem. Int. Ed. 61 (2022) e202201655.

[31] M.E. Simonsen, C. Sønderby, Z. Li, E.G. Søgaard, XPS and FT-IR investigation of silicate polymers, J. Mater. Sci. 44 (2009) 2079–2088.

[32] Y. Ren, X. Lei, H. Wang, J. Xiao, Z. Qu, Enhanced catalytic performance of La-doped $CoMn_2O_4$ catalysts by regulating oxygen species activity for VOCs oxidation, ACS Catal. 13 (2023) 8293–8306.

[33] Z. Ren, H. Qu, A. Wang, Zhao, Acid-etched spinel $CoMn_2O_4$ with highly active surface lattice oxygen species for significant improvement of catalytic performance of VOCs oxidation, Chem. Eng. J. 463 (2023) 142316.

[34] J.-C. Liu, Y. Tang, C.-R. Chang, Y.-G. Wang, J. Li, Mechanistic insights into propene epoxidation with O_2–H_2O mixture on Au_7/α-Al_2O_3: a hydroproxyl pathway from ab initio molecular dynamics simulations, ACS Catal. 6 (2016) 2525–2535.

[35] B.-S. Kim, J. Bae, H. Jeong, C. Choe, H. Lee, Surface restructuring of supported nano-ceria for improving sulfur resistance, ACS Catal. 11 (2021) 7154–7159.

[36] Y. Ma, B. Chi, W. Liu, L. Cao, Y. Lin, X. Zhang, X. Ye, S. Wei, J. Lu, Tailoring of the proximity of platinum single atoms on CeO_2 using phosphorus boosts the hydrogenation activity, ACS Catal. 9 (2019) 8404–8412.

[37] W. Tan, S. Xie, D. Le, W. Diao, M. Wang, K.B. Low, D. Austin, S. Hong, F. Gao, L. Dong, L. Ma, S.N. Ehrlich, T.S. Rahman, F. Liu, Fine-tuned local coordination environment of Pt single atoms on ceria controls catalytic reactivity, Nat. Commun. 13 (2022) 7070.

[38] X. Zhang, Y. Liu, J. Deng, X. Yu, Z. Han, K. Zhang, H. Dai, Alloying of gold with palladium: An effective strategy to improve catalytic stability and chlorine-tolerance of the 3DOM CeO_2-supported catalysts in trichloroethylene combustion, Appl. Catal. B: Environ. 257 (2019) 117879.

[39] M. Wen, F. Dong, J. Yao, Z. Tang, J. Zhang, Pt nanoparticles confined in the ordered mesoporous CeO_2 as a highly efficient catalyst for the elimination of VOCs, J. Catal. 412 (2022) 42–58.

[40] Y. Xi, F. Dong, X. Xu, S. Wu, Z. Tang, J. Zhang, A novel 3D printed technology to construct a monolithic ultrathin nanosheets Co_3O_4/SiO_2 catalyst for benzene catalytic combustion, Nano Res 16 (2023) 12173–12185.

[41] X. Weng, W.L. Wang, Q. Meng, Z. Wu, An ultrafast approach for the syntheses of defective nanosized lanthanide perovskites for catalytic toluene oxidation, Catal. Sci. Technol. 8 (2018) 4364–4372.

[42] S. Wu, S. Wu, F. Dong, Y. Xi, P. Wang, Y. Chu, Z. Tang, J. Zhang, Elucidating the nature role of acid etching on the $CoMnO_x$ catalyst with outstanding performance for the catalytic combustion of o-dichlorobenzene, Appl. Catal. B: Environ. 342 (2024) 123390.

[43] X. Zhao, D. Xu, Y. Wang, Z. Zheng, K. Li, Y. Zhang, R. Zhan, H. Lin, Electric field assisted benzene oxidation over Pt-Ce-Zr nano-catalysts at low temperature, J. Hazard. Mater. 407 (2021) 124349.

[44] J. Hou, J. Hu, L. Chang, J. Wang, Z. Zeng, D. Wu, X. Cui, W. Bao, J. Yao, Synergistic effects between highly dispersed CuO_x and the surface Cu-[O_x]-Ce structure on the catalysis of benzene combustion, J. Catal. 408 (2022) 9–23.

[45] T. Luo, Z. Wang, X. Wei, X. Huang, S. Bai, J. Chen, Surface enrichment promotes the decomposition of benzene from air, Catal. Sci. Technol. 12 (2022) 2340–2345.

[46] X. Ma, M. Xiao, X. Yang, X. Yu, M. Ge, Boosting benzene combustion by engineering oxygen vacancy-mediated Ag/CeO_2-Co_3O_4 catalyst via interfacial electron transfer, J. Colloid Interf. Sci. 594 (2021) 882–890.

[47] L. Li, N. Zhang, R. Wu, L. Song, G. Zhang, H. He, Comparative study of moisture-treated Pd@CeO_2/Al_2O_3 and Pd/CeO_2/Al_2O_3 catalysts for automobile exhaust emission reactions: effect of core-shell interface, ACS Appl. Mater. Interfaces 12 (2020) 10350–10358.

[48] T.-M. Tran-Thuy, C.-C. Chen, S.D. Lin, Spectroscopic studies of how moisture enhances CO oxidation over Au/BN at ambient temperature, ACS Catal. 7 (2017) 4304–4312.

[49] L. Cao, W. Liu, Q. Luo, R. Yin, B. Wang, J. Weissenrieder, M. Soldemo, H. Yan, Y. Lin, Z. Sun, Atomically dispersed iron hydroxide anchored on Pt for preferential oxidation of CO in H_2, Nature 565 (2019) 631–635.

[50] Y. He, F. Guo, K.R. Yang, J.A. Heinlein, S.M. Bamonte, J.J. Fee, S. Hu, S.L. Suib, G. L. Haller, V.S. Batista, In situ identification of reaction intermediates and mechanistic understandings of methane oxidation over hematite: a combined experimental and theoretical study, J. Am. Chem. Soc. 142 (2020) 17119–17130.